Water Air Soil Pollut (2023) 234:297
https://doi.org/10.1007/s11270-023-06303-x

Fabrication of Novel $BiVO_4$ Homostructure with Superior Visible Light Induced Photocatalytic Properties Using Directing Agents

Maira Liaqat · N. R. Khalid

Received: 11 January 2023 / Accepted: 7 April 2023 / Published online: 26 April 2023

Abstract The development of a photocatalyst production through low cost is still a significant concern for locating target material properties and possibility of mass production. Bismuth vanadate ($BiVO_4$) is a semiconductor and mostly used in photocatalysis due to its photocatalytic efficiency in the visible light range. In this research work, a novel synthesis of the $BiVO_4$ photocatalyst was performed using surfactants through a hydrothermal route. Oxalic acid, cetyltrimethyl ammonium bromide (CTAB), and ammonium fluoride (NH_4F) were used as surfactants to maintain crystal orientation, morphology, and greater photocatalytic activity. The synthesized materials were characterized by X-ray diffraction (XRD), scanning electron microscope (SEM), energy dispersive spectroscopy (EDX), UV–Visible spectroscopy (UV–Vis), photoluminescence spectroscopy (PL), Fourier transform infrared spectroscopy (FTIR), and photocatalytic activity. The photocatalytic activity of a prepared sample was investigated via destruction of MB, RhB dye and an antibiotic TC under visible light irradiation. Moreover, it was confirmed that by using XRD and SEM characterization the $BiVO_4/NH_4F$ nanorods exhibited unique morphology and structure. EDX spectroscopy successfully assessed elemental composition of synthesized samples. Optical properties were examined using PL and UV–Visible spectroscopy. The prepared nanorods material degraded almost 77% of MB, 69% of RhB, and 73% of TC in 120 min. The degradation efficiency of $BiVO_4/NH_4F$ material is increased due to the lower recombination rate and enhanced production of a number of defects and oxygen vacancies.

Keywords Hydrothermal method · Photocatalytic degradation · MB · RhB · TC · Rod-like nanostructure

Highlights
- $BiVO_4$ using surfactants as photocatalysts were fabricated via the hydrothermal method for the degradation of MB, RhB and TC.
- $BiVO_4/NH_4F$ nanorods have shown 77% degradation activity against MB pollutants.
- $BiVO_4/NH_4F$ nanorods show high stability.
- The enhanced performance was ascribed to facilitate photogenerated charge carriers and also enhanced the adsorption of molecules.

M. Liaqat (✉)
Department of Physics, University of Gujrat, Hafiz Hayat Campus, Gujrat 50700, Pakistan
e-mail: mairawarraich88@gmail.com

N. R. Khalid
Department of Physics, University of Okara, Okara, Pakistan

1 Introduction

For the survival of all kinds of animals and living organisms, clean water is an important factor. Our earth consists of 70% water but a minimum amount of 2.5% water is used for agriculture, drinking, industrial and domestic utilization. From the

twenty-first century, water pollution, environmental pollution and global warming spread diseases, change our climate and create many problems for the survival of all kinds of life. Nowadays, environmental safety and remediation become major challenges for all mankind. Many industrial sectors like dyeing, printing, plastic, paper, cosmetics, ink, textiles ceramics, leather sectors and food processing release huge amounts of sewage and toxicity materials (Lotfi, 2022; You et al., 2019). According to survey, these industries release one thousand tons of waste material which consists of non-biodegradable dye stuff. Hence, it is very crucial to clean water for the protection of the environment and life. To overcome this problem, semiconductor photocatalysis has been observed eco-friendly because it has many properties such as being cost-effective, sustainable and non-toxic with greater photostability (Cheng et al., 2020; Kaur et al., 2020; Malathi et al., 2018).

These days, researchers have focused their research on two ways. The first way is by preparing a photocatalyst that will be able to utilize visible light which covers more than 50% of the solar spectrum. The second way is by improving the productivity of the photocatalytic reaction through adjusting synthesis conditions, using structure directing agent or producing new synthesizing methods (Deebasree et al., 2020). Nowadays, more than 150 semiconductor materials are developed for the cleanliness of water and environmental pollution (Kaur et al., 2020). Beyond these prepared semiconductors titanium dioxide, zinc oxide, bismuth, and bismuth vanadate based semiconductors (Bhowmick, et al., 2019; Kumar et al., 2018; Luo et al., 2022a) are considered as the best photocatalysts due to their different properties and multifunctional applications such as ionic conductivity, ferroelasticity, acousto optical photocatalytic activity, less toxicity, strong oxidizing power, greater stability, low cost, narrow band gap, gas sensor devices, lead-free paints, solid state electrolytes and lithium ion batteries, etc. (Aghakhaninejad et al., 2018; Ghotekar et al., 2020; Helal, et al., 2020; Jia et al., 2012; Kása et al., 2020; Luo et al., 2022b; Wu et al., 2018; Zhang et al., 2021; Zhong et al., 2023). TiO_2 is considered as a useful material for many photocatalytic applications. The main drawback of TiO_2 is its large bandgap, i.e. 3.2 eV, which needs ultraviolet light for photocatalytic activation (Chang & Liu, 2011; Zhang et al., 2014). The excellent properties of $BiVO_4$ are resistance to corrosion, best dispersibility, non-toxicity, and long-term photostability (Choi et al., 2013; Zhang & Zhang, 2009).

The n-type semiconductor bismuth vanadate has good crystallinity and morphology. There are three types of polymorphs such as monoclinic scheelite, tetragonal scheelite and tetragonal zircon. Tetragonal scheelite is a natural polymorph also called pucherite and it has orthorhombic crystal structure. The dreyerite polymorph has tetragonal scheelite structure and the clinobisvanite has monoclinic scheelite structure. The tetragonal scheelite was not prepared by simple laboratory method but the monoclinic scheelite and tetragonal zircon can be prepared. At higher temperatures, tetragonal zircon can be changed into monoclinic scheelite. The reversible transition in $BiVO_4$ tetragonal scheelite to $BiVO_4$ monoclinic scheelite can be found at temperature 528 K (Trinh et al., 2019). The structure of monoclinic scheelite is considered a strong reactive phase due to its bandgap 2.4–2.5 eV (Chen et al., 2020; Helal, et al., 2020; Hemavibool et al., 2022; Hunge et al., 2021). In monoclinic scheelite, the transition in valance band is made by Bi_6 or due to the hybrid orbital of O_{2p} and Bi_6 to a conduction band of V_{3d} (Jiang et al., 2012, 2014; Li et al., 2016). Thus, in the monoclinic phase, smaller band gaps have appropriate band positions of conduction and valance band. These bands are almost near to H_2O reduction and oxidation potential (Rani et al., 2019; Tayebi & Lee, 2019; Wu et al., 2021). Hence, the band gap and band position help $BiVO_4$ crystal to absorb maximum visible light. Due to these characteristic, $BiVO_4$ shows a stronger visible light–driven photocatalytic properties in case of water splitting, removal of organic pollutants, and photocatalytic O_2 evolution (Kshetri et al., 2020; Senasu et al., 2021). The main disadvantage found in $BiVO_4$ photocatalysts is fast recombination of photogenerated charge carriers in conduction band and valance band. To overcome this problem, scientists prepare different heterojunction photocatalysts (Nguyen, 2020).

Researchers use a variety of structure directing agents also called surfactants for preparing different kinds of semiconductors (Monfort & Plesch, 2018). The main advantage of adding surfactants in precursor solution is that, it will produce many changes in materials and played an important role for improving band gap, crystal structure, morphology, electron

hole pair recombination, electron mobility, photocatalytic activity and develop a stable environment for growth kinetics of nanomaterials in different synthesis processes (Rani et al., 2018). Hence, the benefits of surfactants in synthesis process of nanostructure materials show the greater surface area, change in morphology, thin pore size, porosity, crystal phase formation and high crystallinity etc. (Afonso et al., 2014).

Furthermore, Yidan Luo et al. synthesized NiAl-LDH/biochar nanocomposites using the coprecipitation method. It was observed that, S-scheme heterojunction was found between NiAl-LDH and biochar. This junction enhanced the separation of photogenerated electrons and holes. The photogenerated electrons and holes increased photocatalytic activity. Due to greater photocatalytic activity, NiAl-LDH/biochar was considered the best photocatalyst and removes antibiotics from water (Luo et al., 2022b).

Monoclinic bismuth vanadate powder was synthesized through the hydrothermal method by Rong Ran et al. He observed that a bismuth vanadate catalyst shows better photocatalytic activity for the degradation of RhB dye i.e. 88% in 120 mint. This dye shows greater removal capacity (Ran et al., 2015). Yidan Luo et al. prepared bismuth oxychloride/biochar (BiOCl/BC) nanocomposites with abundant oxygen vacancies through the facile ball milling technique. These composites have superior adsorption for the removal of reactive red-120 dye in aqueous solution. It was observed that a strong interaction is found between BiOCl and BC after ball milling (Luo et al., 2022a).

Novel composites of the $BiVO_4/Bi_2O_3$ heterostructure were fabricated through the hydrothermal technique. These composites show superior photocatalytic activity for RhB dye and TC under visible light irradiation. It was observed that 5% $BiVO_4/Bi_2O_3$ catalyst have excellent photocatalytic activity as compared to other materials. The RhB dye degradation rate was almost 79%, while TC degrades 74%. This enhanced photocatalytic activity was due to p-n heterojunction (Liaqat et al., 2022).

Ch. Venkata Reddy et al. designed novel g-C_3N_4/$BiVO_4$ heterostructured nanohybrids through the solvothermal technique. The photocatalytic activity of g-C_3N_4/$BiVO_4$ was examined through MB and TC i.e. 88% and 89%. The enhanced catalytic performance was due to heterojunction between g-C_3N_4 and $BiVO_4$. It was observed that these prepared composites of g-C_3N_4/$BiVO_4$ are also suitable for environmental remediation applications (Reddy, et al., 2023).

Here, in this research work we have explained photocatalytic activity and morphology of $BiVO_4$ nanostructures using surfactants through the hydrothermal route. To the best of our knowledge, this is the first report with respect to synthesis of monoclinic $BiVO_4/NH_4F$. It was also observed that ammonium fluoride (NH_4F) is a good surfactant as a morphology controlling agent, enhancing optical properties of the prepared catalyst and photocatalytic activity. The prepared photocatalysts are most suitable for degradation of model organic dyes (MB and RhB) and tetracycline hydrochloride.

2 Experimental Procedures

2.1 Materials for Preparation

Bismuth nitrate ($Bi(NO_3)_3{\cdot}5H_2O$), ammonium metavanadate (NH_4VO_3), ethanol, ammonium fluoride, oxalic acid, CTAB, sodium hydroxide, nitric acid, acetone, methylene blue, Rhodamine B, tetracycline hydrochloride, and deionized water were utilized to fabricate desired materials. All chemicals and reagents were pure and directly used without performing any modifications.

2.2 Synthesis of Pure and Surfactant-Based $BiVO_4$ Material

First of all, we dissolve 5 mmol of NH_4VO_3 into ethanol and stirred at 50 °C for 30 min. Then 5 mmol of $Bi(NO_3)_3{\cdot}5H_2O$ was dissolved into ethanol and stirred at 50 °C for 30 min. Then by using burette add NH_4VO_3 solution dropwise into $Bi(NO_3)_3{\cdot}5H_2O$ solution, and both mixtures were stirred continuously for 2 h during stirring add a little quantity of surfactants individually (ammonium fluoride, oxalic acid, and CTAB). The pH ~ 8 of this solution was maintained by using 50 vol. % NaOH and HNO_3. After that, the whole mixture was poured into a Teflon-lined autoclave for hydrothermal synthesis at 180 °C for 12 h. Then, the obtained precursor was washed through deionized water, acetone and two times with ethanol. Hence, the washed material was put into a drying oven at 80 °C for 12 h. After drying, the whole

material was calcined at 550 °C. At the end, the prepared material was collected to characterize and do photocatalytic tests. The pure $BiVO_4$ was also prepared using the same procedure without adding surfactants. The schematic flowchart for preparation of $BiVO_4$ using surfactants is displayed in Fig. 1.

2.3 Characterization of Photocatalysts

The phase structure of as-synthesized nanomaterials were explored by the powder X-ray diffraction machine through D/max 2500 having CuKα source ($\lambda = 0.1541$ nm). A scanning electron microscope (SEM; LEO 1530) was used to distinguish structural properties such as morphology and elemental composition of as-synthesized photocatalysts. For examining the UV–Visible absorption spectra of the photocatalysts, the UV-1800 spectrometer by Shimadzu was used. JASCO fluorescence spectrometer with FP-8200 was used to determine the photoluminescence spectra (PL) at a fixed excitation wavelength i.e. 400 nm for all prepared photocatalysts.

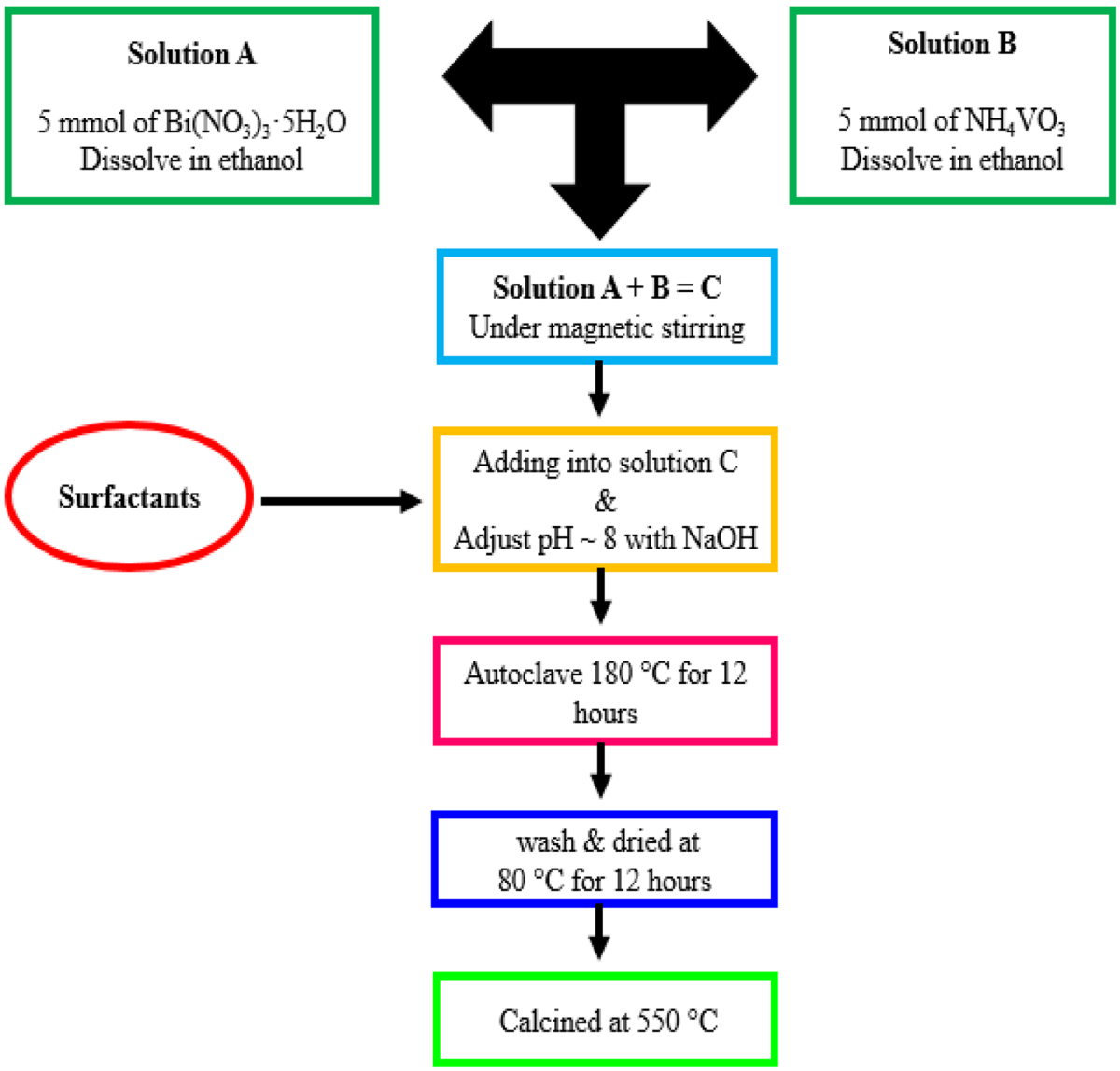

Fig. 1 Flowchart for synthesis of $BiVO_4$

Moreover, the FTIR spectroscopy measurements were used to investigate the prepared composites.

2.4 Photocatalytic Degradation Study

MB dye, RhB dye and antibiotic TC were used to examine the photocatalytic activity of prepared $BiVO_4$ in a liquid medium through visible light irradiation. A photocatalytic reactor was used in photocatalytic experiments, consisting of tungsten halogen lamps (50 W per lamp) as a source of visible light. For checking photocatalytic activity, 20 mg of as-synthesized material was dissolved in 100 mL of MB solution i.e. 10 mg L^{-1} in a Pyrex glass vessel having pH of MB solution as almost 10. After that for attaining adsorption or desorption equilibrium on photocatalyst surfaces, the whole mixture was stirred about half an hour. After stirring, the whole solution took place at 15 cm away from the lamp and irradiation was started with light of lamp having wavelength range larger than 420 nm using a filter. After each half hour, 5 mL solution was taken from the reactor vessel. The prepared solution was centrifuged and concentration of dye degradation was measured by the UV–Visible spectrometer UV-1800 by Shimadzu. Hence, the whole procedure was repeated for RhB dye and TC.

3 Results and Discussion

3.1 Structure and Phase Identification

The crystalline phase structures of $BiVO_4$ using surfactants were determined through X-ray diffractometer (D/max 2500) using Cu-kα radiation having wavelength 1.5406 Å. Figure 2a display XRD patterns of as-synthesized pure $BiVO_4$ using the hydrothermal method. The diffraction peaks were observed at 2θ angles 19°, 27.48°, 28.26°, 31.64°, 34.75°, 35.64°, 45.0°, 46.78°, 47.55°, 55.31° and 57.34° corresponding to hkl values of (011), (− 121), (121), (113), (200), (002), (123), (240), (042), (206), (125), (321) and (134) respectively according to JCPDS Nos. 14–0688 and 14–0133. The largest peak at 28.26° shows maximum crystallinity and monoclinic structure with respect to other peaks. Figure 2b shows XRD pattern of $BiVO_4$ using oxalic acid as a surfactant. Diffraction peaks observed in XRD patterns can be indexed as (101), (011), (013), (040), (002), (211), (051), (123), (240), (042), (202), (161), (321) and (134) at 2θ angles 18.84°, 19°, 29.02°, 30.0°, 35.64°, 39.87°, 42.56°, 45°, 46.78°, 47.55°, 50°, 53.0°, 58.54° and 59.88° respectively which show a pure monoclinic scheelite phase according to JCPDS No. 75–2480 and JCPDS No. 14–0688 (Kása et al., 2020; Wang et al., 2014). Figure 2c describe XRD pattern of $BiVO_4$ using ammonium fluoride as a surfactant. The observed diffraction peaks at 2θ angles 11.04°, 19°, 27.48°, 28.26°, 29.02°, 31.64°, 35.64°, 37.12°, 40.94°, 42.56°, 45.0°, 46.78°, 49.28°, 53.0°, 55.31°, 58.54°, 59.88° and 61° corresponding to hkl values of (001), (011), (− 121), (121), (013), (113), (002), (141), (105), (051), (123), (240), (312), (161), (125), (321), (134) and (332) respectively. $BiVO_4$ using surfactant ammonium fluoride shows narrow line widths and higher degree of crystallinity (Dabodiya et al., 2019; Sivakumar et al., 2015). This monoclinic scheelite phase is considered as a more active phase as compared to other phases of $BiVO_4$. Figure 2d observed the XRD pattern of $BiVO_4$ using CTAB as a surfactant. The detected diffraction peaks at 2θ angles 11.04°, 19°, 25.32°, 29.02°, 30.0°, 31.64°, 34.75°, 35.64°, 39.87°, 42.56°, 46.78°, 47.55°, 50°, 53.0°, 57.34°, 58.54° and 59.88° corresponding to hkl values of (001), (011), (111), (013), (040), (113), (200), (002), (211), (051), (240), (042), (202), (161), (206), (321) and (134) respectively. During calcination at high temperatures i.e. 550 °C peak at 35.20° splits into two other diffraction peaks (200) at (34.75°) and (002) at (35.64°). Two diffraction peaks show tetragonal phase of $BiVO_4$ having hkl values (111) and (200) with respect to JCPDS 14–0133 (Brack, et al., 2015; Cheng et al., 2013; Khan, et al., 2020). These observed peaks prove that prepared material is a mixture of monoclinic and tetragonal $BiVO_4$ (Cheng, 2012; Khan et al., 2020; Zhang et al., 2007). Hence by preparing $BiVO_4$ using surfactants, it was concluded that all prepared materials are pure without finding any impurity of other materials' diffraction peaks for example Bi_2O_3 and V_2O_5. Furthermore, it was concluded that XRD peak intensity of monoclinic $BiVO_4$ was stronger as compared to tetragonal $BiVO_4$ and FWHM of monoclinic $BiVO_4$ diffraction peaks are little narrow or decreased and prove

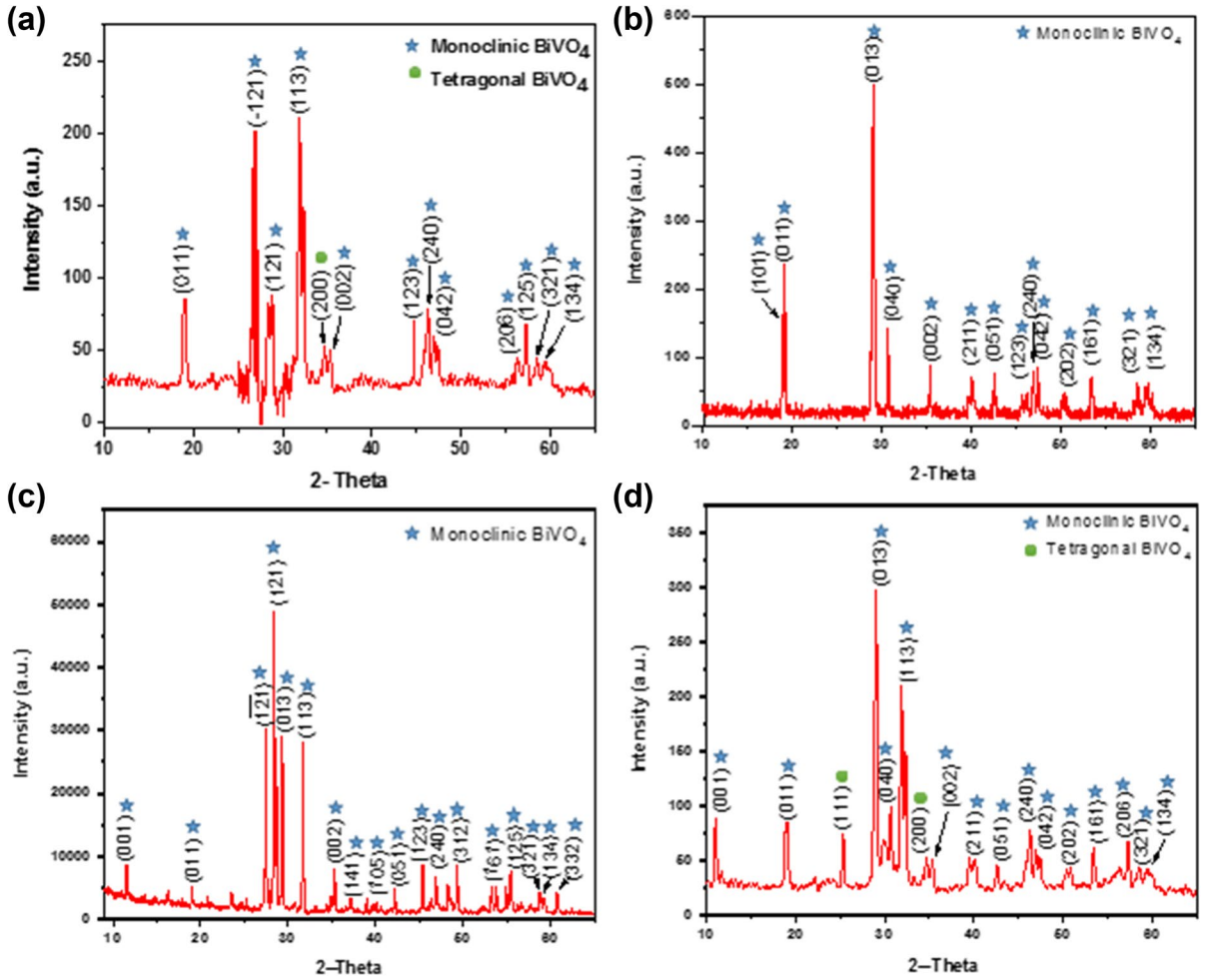

Fig. 2 XRD results of pristine $BiVO_4$ (**a**), $BiVO_4$/oxalic acid (**b**), $BiVO_4/NH_4F$ (**c**) and $BiVO_4$/CTAB (**d**)

Table 1 Detail of XRD

Sr. #	Material name	Crystal size (nm)	Crystallinity index	Nature of crystal
1	Pure $BiVO_4$	25.07	78.53	Monoclinic
2	$BiVO_4$/oxalic acid	27.57	80.75	Monoclinic
3	$BiVO_4$/CTAB	27.32	79.62	Monoclinic
4	$BiVO_4$/ammonium fluoride	28.47	82.05	Monoclinic

that higher crystallinity and maximum $BiVO_4$ crystallites. Table 1 describes the detail of XRD such as crystal size, crystallinity index and nature of all prepared samples.

3.2 SEM and EDX Characterization

The morphologies of $BiVO_4$ samples synthesized through hydrothermal route were characterized by using high-resolution scanning electron microscope (SEM; LEO 1530). Figure 3a–d explain the

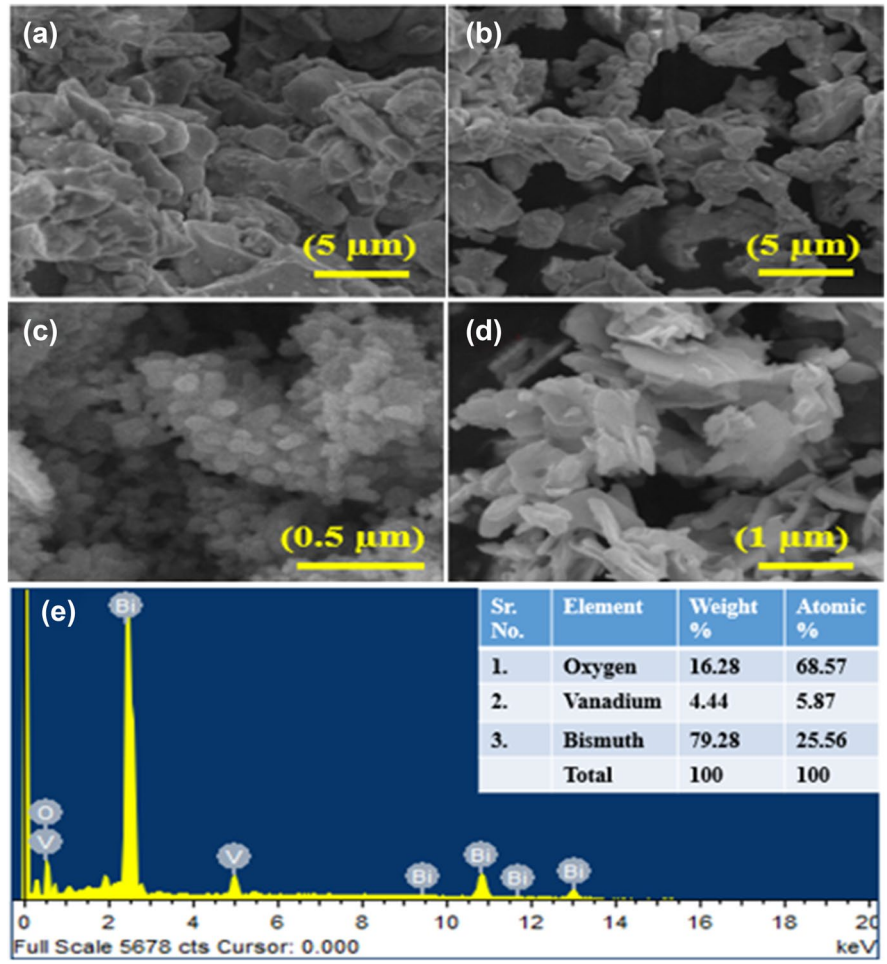

Sr. No.	Element	Weight %	Atomic %
1.	Oxygen	16.28	68.57
2.	Vanadium	4.44	5.87
3.	Bismuth	79.28	25.56
	Total	100	100

Fig. 3 SEM images of pristine $BiVO_4$ (**a**), $BiVO_4$/oxalic acid (**b**), $BiVO_4$/CTAB (**c**), $BiVO_4/NH_4F$ (**d**) and EDX spectra of $BiVO_4$ (**e**)

morphologies of pristine $BiVO_4$ and surfactant-based $BiVO_4$ samples. Prepared samples show that there are major differences in the morphologies and particle shapes of $BiVO_4$ using surfactants. As revealed in Fig. 3a and b the morphology of pure $BiVO_4$ and $BiVO_4$ using oxalic acid is agglomerated. Figure 3c describes the morphology of $BiVO_4$ using CTAB as a surfactant. By using CTAB as a surfactant, the morphology of $BiVO_4$ totally changed and nanoparticles were found. The average length of nanoparticles is 49.49 nm, while the mean diameter range of these nanoparticles is 36.05 nm. Interestedly, it can be seen that when surfactant ammonium fluoride was used nanorods will be as shown in Fig. 3d. The mean length and diameter of nanorods are 81.31 nm and 21.82 nm. These nanorods explain better results as compared to other surfactants (Helal, et al., 2020).

For further confirmation of synthesis of $BiVO_4$, the elemental composition of $BiVO_4$ was examined via energy dispersive spectroscopy. Figure 3e illustrates the EDX analysis of $BiVO_4$ and calculated atomic ratios of Bi, O, and V are 2:3:1. Hence, the presence of bismuth, vanadium and oxygen are clearly evidences of the formation of $BiVO_4$ and the absence of any other impurity proves the highly pure nature of $BiVO_4$.

3.3 UV–Visible Spectroscopy Analysis

In semiconductors, the optical absorption property has a greater role in photocatalytic performance. Optical properties of characterized samples were examined through a UV-1800 spectrometer by Shimadzu. The results of UV–Visible spectroscopy are displayed in Fig. 4a and b. The light absorption ranges of all characterized photocatalysts have 300–800 nm. This range is

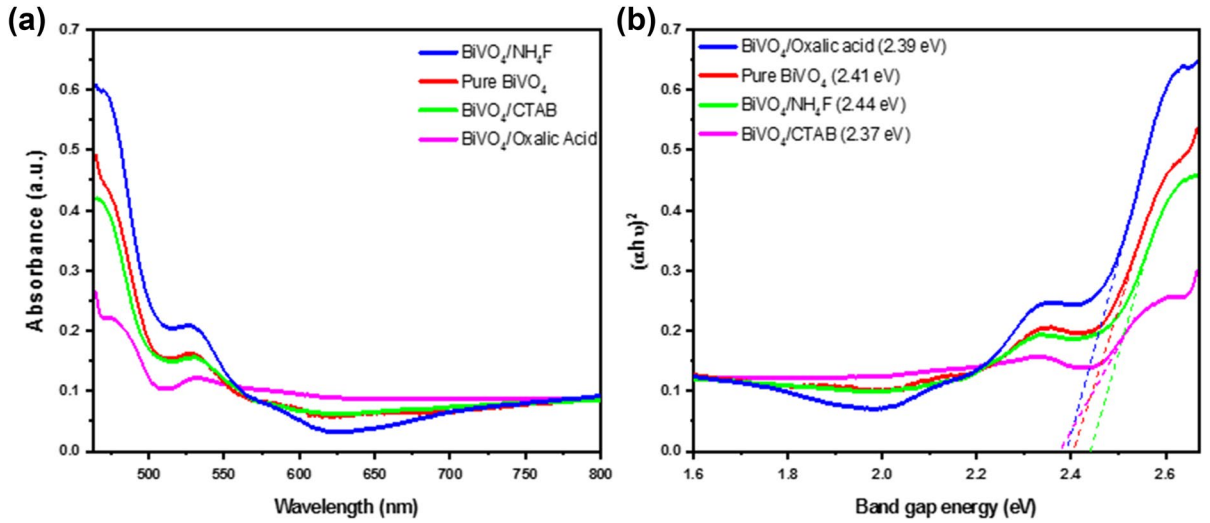

Fig. 4 UV–Visible absorption spectra of $BiVO_4$ using surfactants (**a**) and Plot of $(\alpha h\upsilon)^2$ vs hυ of $BiVO_4$ using surfactants (b)

displayed in Fig. 4a and describes that all synthesized samples have good capability to absorb UV–Visible light and also have potential of photocatalysis in visible light. The absorption edge of all prepared samples are in green shift (Zhang et al., 2020). The maximum absorption in visible light region is produced because of the transfer of electrons from Bi 6 s and O 2p orbitals to V 3d orbitals (Ahmed et al., 2018).

In semiconductors, band gap values can be calculated with the help of Tauc relationship:

$$\alpha h\upsilon = A(h\upsilon - E_g)^{\frac{n}{2}} \quad (1)$$

By using Tauc formula, a plot of $(\alpha h\upsilon)^2$ versus (hυ) is displayed in Fig. 4b.

The calculated band gaps of pure $BiVO_4$, $BiVO_4$/oxalic acid, $BiVO_4$/CTAB and $BiVO_4/NH_4F$ were estimated to be 2.41, 2.39, 2.37 and 2.44 at wavelengths 514 nm, 518 nm, 523 nm and 508 nm respectively. These band gap values are related with literature reports of the $BiVO_4$ monoclinic structure (García-Pérez et al., 2012; Lin et al., 2019; Mousavi-Kamazani, 2019; Yu & Kudo, 2006; Zhou et al., 2006, 2007). The better optical properties of $BiVO_4/NH_4F$ composites in visible light range are the best sign of their photocatalytic performance.

3.4 Photoluminescence Analysis

A photoluminescence spectroscopy is an appropriate method to observe the recombination rate, transfer capacity, trapping mechanism, separation of photogenerated charge carriers and oxygen defects. Lower PL intensity shows reduction in electron hole pair recombination rate and greater photocatalytic activity (Cheng et al., 2020). PL spectra illustrated in Fig. 5 were recorded by JASCO fluorescence spectrometer with FP-8200. The $BiVO_4$ using surfactants was excited by 400 nm and three predominant emission peaks were obtained (Rani et al., 2019). These peaks situated in the blue region have wavelengths at

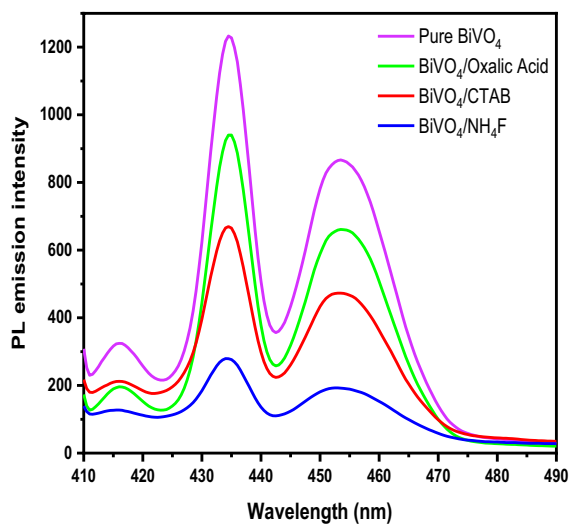

Fig. 5 Photoluminescence spectra of $BiVO_4$ using surfactant

416 nm, 434 nm, and 453 nm. The decreasing order of PL intensity of prepared $BiVO_4$ using surfactants is $BiVO_4/NH_4F < BiVO_4/CTAB < BiVO_4/$oxalic acid < pure $BiVO_4$. The decrease in PL intensity of prepared samples show greater photocatalytic activity. Here, luminescence spectra produced through the emission of photons are produced due to the recombination of holes in O 2p orbital band and photo excitation of electrons in V 3d orbital band. The PL results relate with energy band diagram which proves low recombination and good photocatalytic activity. Ammonium fluoride shows the best photocatalytic activity because the recombination rate is too slow as compared to other surfactants. Hence, the PL results conclude that the surfactants produce a significant role for improving photoelectron hole pair separation in $BiVO_4$ and enhanced its photocatalytic performance (Liu et al., 2018).

3.5 FTIR Analysis

To examine the chemical structure and bands of $BiVO_4$ using surfactants, the FTIR spectra were used (Benisti et al., 2020). The spectra of $BiVO_4$ using surfactants are illustrated in Fig. 6. In pure $BiVO_4$ absorption band at 700 – 900 cm^{-1} is due to symmetric and asymmetric stretching vibrations of V – O bond. The peak at value of 698 cm^{-1} demonstrates the Bi – O bond while at 733 cm^{-1} stretching peaks relate with vanadium. The absorption band at 741 cm^{-1} shifted at 737 cm^{-1}, while absorption band at 829 cm^{-1} also shows symmetric stretching of $(VO_4)^{3-}$. Hence, the peaks at 829 cm^{-1} and 831 cm^{-1} are due to variations in particle sizes and metal ion oxygen bond distance during calcination temperature.

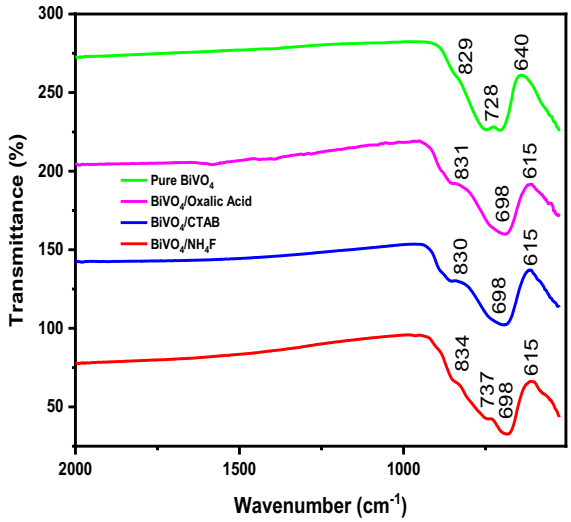

Fig. 6 FTIR spectra of $BiVO_4$ using surfactant

3.6 Photocatalytic Activity

The photocatalytic activity of $BiVO_4$ using surfactants was calculated by using methylene blue and RhB model organic dyes in sunlight. The degradation efficiency was calculated with the help of formula i.e.

$$Degradation\ efficiency(\%) = \frac{C_o - C}{C_o} \times 100 \quad (2)$$

Here, C_o called initial concentration and C called final concentration of MB and RhB dye. Figure 7a and b demonstrate that no methylene blue and RhB degradation could be found in blank treatment (without catalyst) through visible light illumination. But Fig. 7c and d explain the percentage degradations of MB for prepared pristine $BiVO_4$, $BiVO_4$/oxalic acid, $BiVO_4$/CTAB and $BiVO_4/NH_4F$ are 42%, 47%, 59% and 77% while for RhB the degradation percentages of pristine $BiVO_4$, $BiVO_4$/oxalic acid, $BiVO_4$/CTAB and $BiVO_4/NH_4F$ are 48%, 54%, 61% and 69% within 2 h of irradiation time. Table 2 describes the comparison of photocatalytic activity of synthesized $BiVO_4$ photocatalyst with reported literature.

3.7 Kinetic Study of $BiVO_4$ Using Surfactants

The photocatalytic activity against MB and RhB dye can also be determined by using pseudo first-order reaction kinetics. For $BiVO_4$-based photocatalyst, the degradation rate constant, i.e. k, was determined by using formula, i.e. $\ln(C_o/C) = kt$. The pseudo first-order reaction kinetics and k values for pristine $BiVO_4$, $BiVO_4$/CTAB, $BiVO_4$/oxalic acid and $BiVO_4/NH_4F$ in case of MB and RhB are displayed in Fig. 8a–d. These k values were estimated with the help of slopes calculated between $\ln(C_o/C)$ vs. time. The calculated apparent constant values by using MB dye for prepared pristine $BiVO_4$, $BiVO_4$/oxalic acid, $BiVO_4$/CTAB and $BiVO_4/NH_4F$ are 0.0038 min^{-1}, 0.0051 min^{-1}, 0.0070 min^{-1} and 0.0103 min^{-1} but by using RhB dye values are 0.0036 min^{-1},

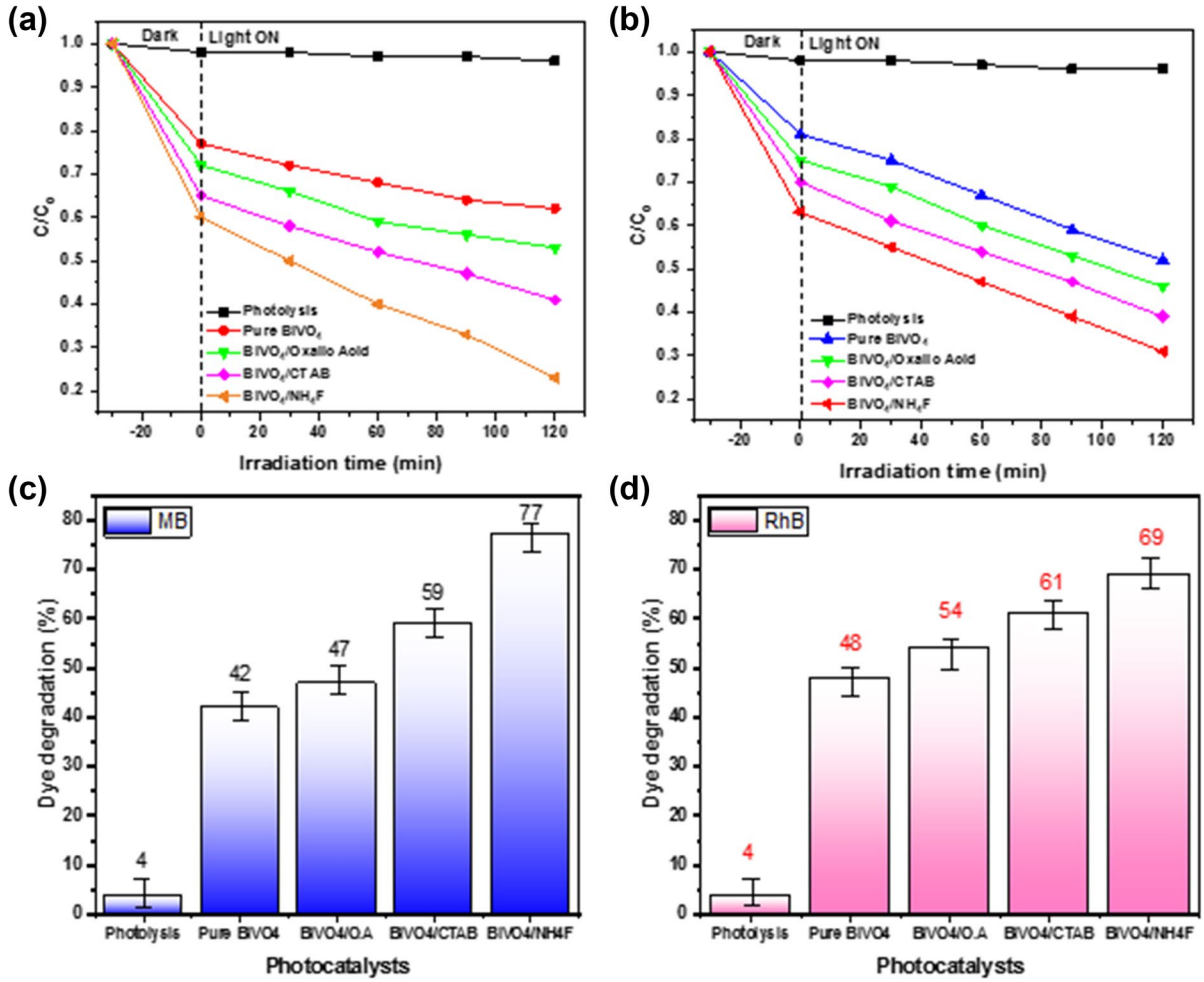

Fig. 7 Photocatalytic activity comparison of different photocatalysts for MB dye degradation (**a**), RhB dye degradation (**b**), MB dye degradation percentage (**c**) and RhB dye degradation percentage (**d**)

0.0043 min^{-1}, 0.0059 min^{-1} and 0.0067 min^{-1}. By comparing methylene blue and rhodamine B, it was observed that the kinetics value of $BiVO_4/NH_4F$ is greater in case of methylene blue as compared to RhB. This may be due to many reasons such as the chemical structure, adsorption characteristics and susceptibility to degradation of both dyes is different.

Moreover, tetracycline antibiotic pollutant was also used to overcome the effect of dye self-sensitization. Figure 9a exhibits photocatalytic ability of $BiVO_4$-based photocatalysts for TC degradation through visible light exposure. There is 50% of TC that could be removed through pristine $BiVO_4$ photocatalyst after irradiation time of 2 h. It was also observed that the $BiVO_4$ using surfactants showed better photocatalytic efficiency and $BiVO_4/NH_4F$ exhibited outstanding efficiency, i.e. 73% as compared to other synthesized materials. Figure 9b describes photocatalytic degradation percentage of TC. Additionally, the pseudo first-order reaction kinetics and kinetic constant values of pristine $BiVO_4$, $BiVO_4$/oxalic acid, $BiVO_4$/CTAB and $BiVO_4/NH_4F$ were 0.0046 min^{-1}, 0.0058 min^{-1}, 0.0072 min^{-1} and 0.0098 min^{-1} respectively which are displayed in Fig. 9c and d.

3.8 Stability Test of $BiVO_4$ Using Surfactants

To calculate the performance at the commercial level of as-prepared $BiVO_4/NH_4F$ photocatalysts, the

Table 2 Comparison of photocatalytic activity of synthesized $BiVO_4$ photocatalysts with reported literature

Photocatalyst	Dye	Time (min)	Efficiency (%)	Reference
$BiVO_4$	MO	240	97.8	Mao et al., 2020)
$MoO_3/BiVO_4$	MB	120	76	Liaqat & Khalid, 2021)
Ni-doped $BiVO_4$	RhB	75	96	Li et al., 2020)
m-$BiVO_4$	MB	30	97	Ahmed et al., 2018)
$BiVO_4$	MB	120	92.25	Ganeshbabu et al., 2020)
Bi_2O_3/ $BiVO_4$	Tetracycline	120	74	Liaqat et al., 2022)
$BiVO_4$	RhB	180	90.08	Chen et al., 2020)
$MnO_2/BiVO_4$	RhB	120	87	Liaqat et al., 2023)
$BiVO_4$	MB	105	97	Sivakumar et al., 2015)
$BiVO_4$	Thiophene	180	81	Mousavi-Kamazani, 2019)
$Bi_2O_2CO_3$	Tetracycline	60	84.7	Luo et al., 2023)
$BiVO_4$	Crystal violet	90	99.1	Sajid et al., 2020)
$BiVO_4/NH_4F$	RhB MB TC	120	69 77 73	Present work

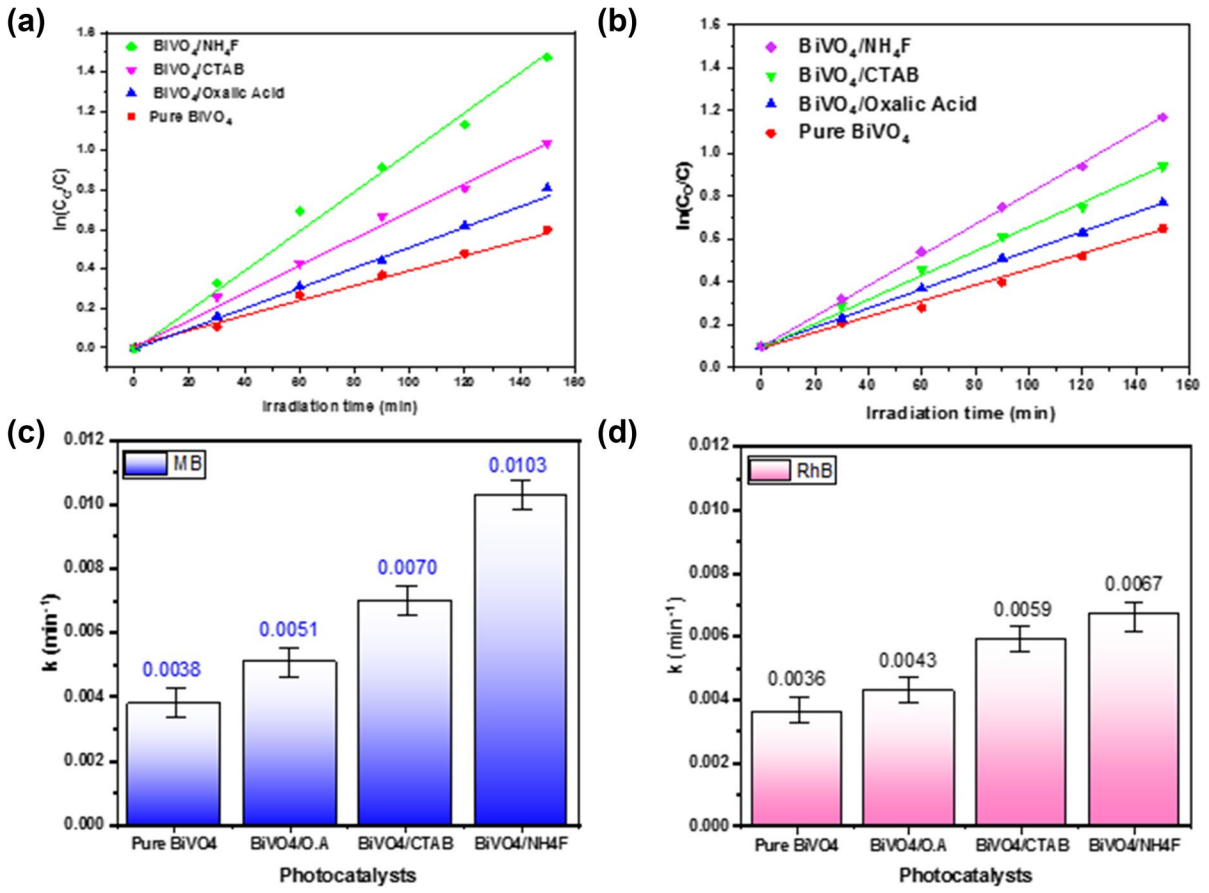

Fig. 8 Plot of ln (C_O/C) versus irradiation time for MB dye degradation (**a**), RhB dye degradation (**b**), kinetic curves of MB degradation (**c**) and kinetic curves of RhB degradation (**d**)

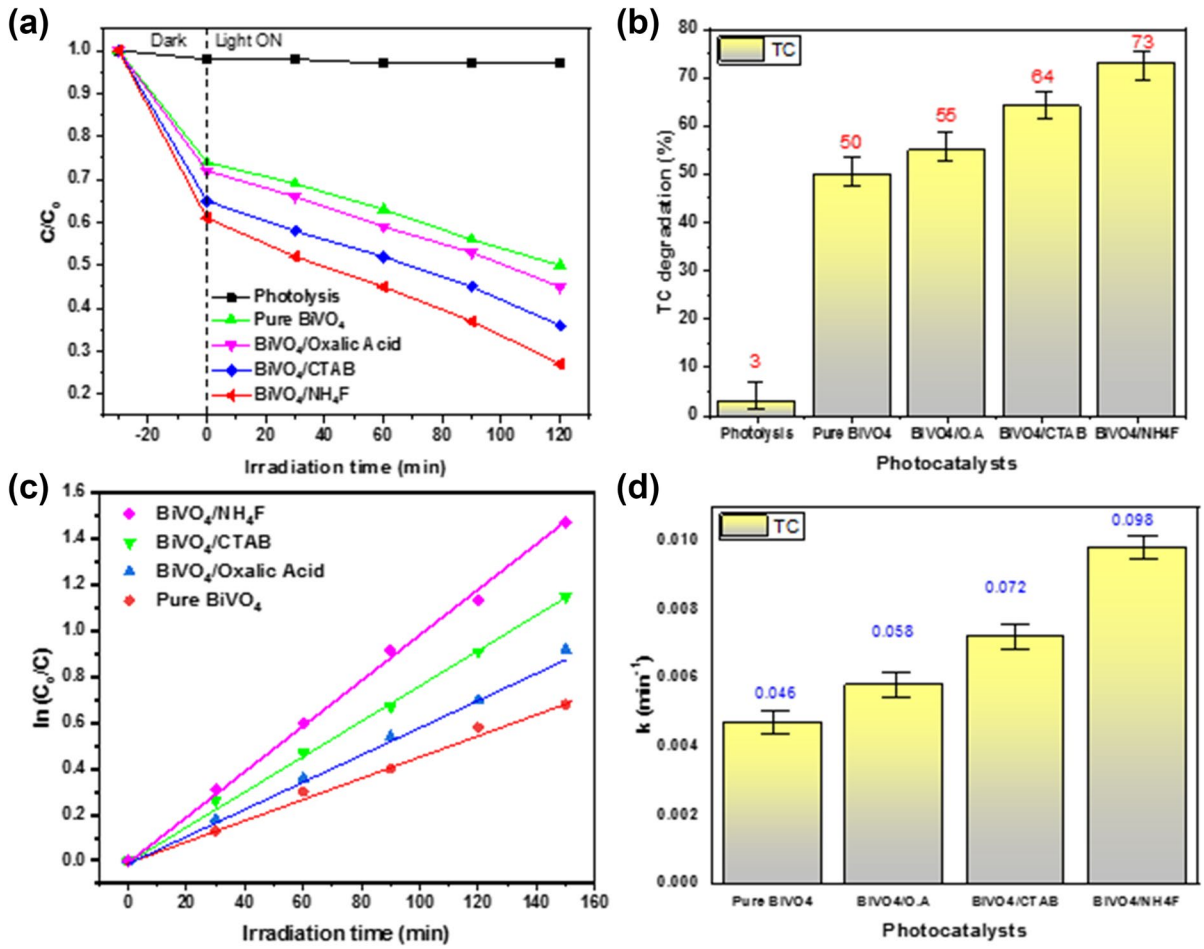

Fig. 9 Photocatalytic degrading TC solution curve of $BiVO_4$ using surfactants (**a**), TC degradation percentage (**b**), pseudo first-order reaction kinetics of $BiVO_4$ using surfactants (**c**) and kinetic curves of TC degradation (**d**)

stability and reusability tests were done through the same parameters and conditions as for model pollutant MB degradation (described in Sect. 2.4). The obtained results are illustrated in Fig. 10a. These results examine that there was a minor reduction in $BiVO_4/NH_4F$ after consecutive five cycles. These cycles prove the stability of $BiVO_4/NH_4F$ as a novel photocatalyst. Furthermore, for more clarification of the stability and reusability of $BiVO_4/NH_4F$ photocatalysts, XRD characterization was performed before and after the degradation process. The results of XRD characterization are displayed in Fig. 10b. It could be found that no new peaks came out before and after the reaction indicating that $BiVO_4/NH_4F$ was not changed. These XRD results also explain that the $BiVO_4/NH_4F$ photocatalysts have good stability, more efficient, economic, and have a large potential in industrial applications.

3.9 Effect of Radical Scavenger

A radical trapping experiment was achieved to elucidate the as-involved active species which are responsible for degradation of model organic MB dye. In the radical trapping experiment, the radical scavengers like ethylenediaminetetraacetate, tert-butyl alcohol and 1,4-benzoquinone were used. This experimental method was like the degradation experiment discussed in Sect. 2.4 with addition of 1 mmol of quenchers EDTA, t-BuOH and BQ in the presence of aqueous solution MB. The obtained results are displayed in Fig. 10c. It was observed that due to addition

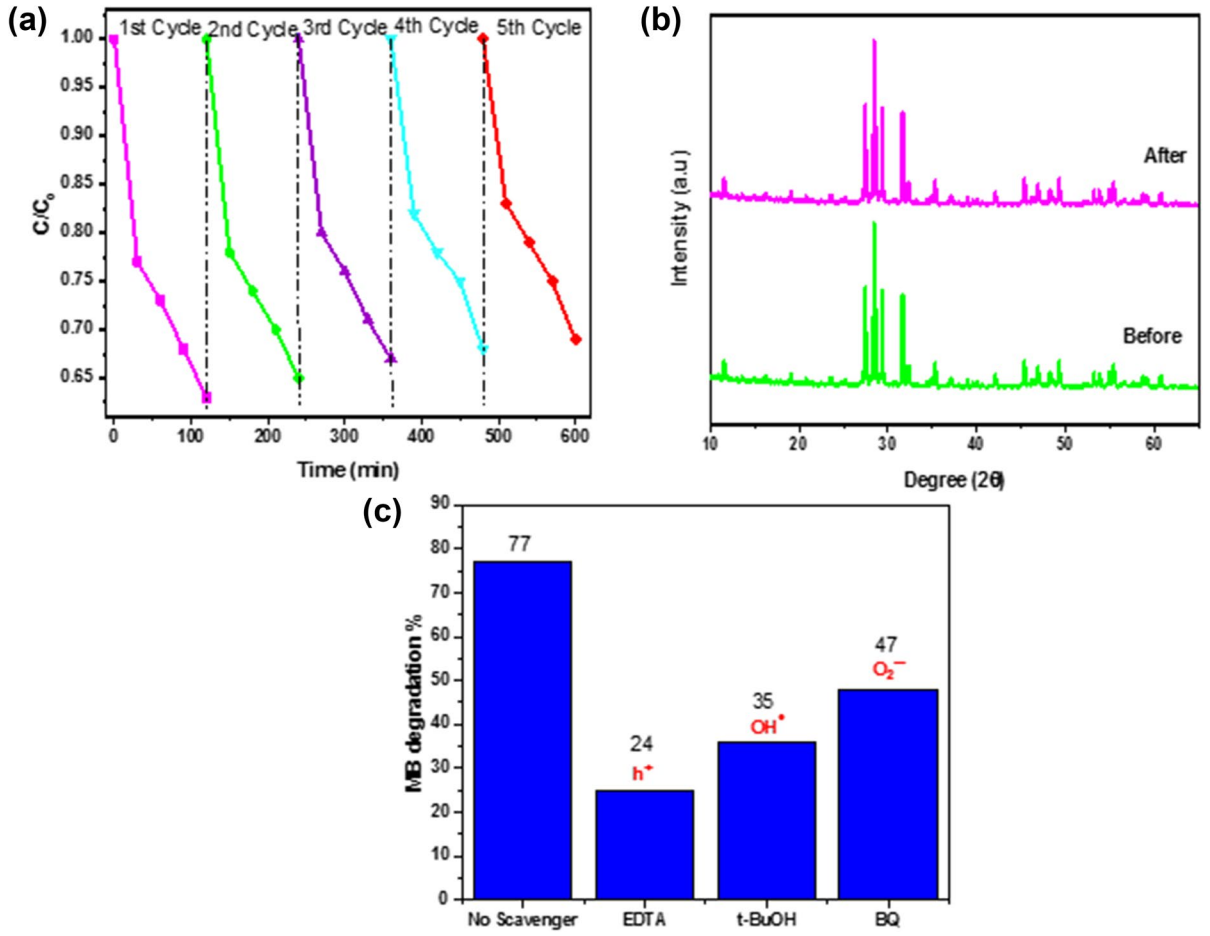

Fig. 10 Reusability test of $BiVO_4/NH_4F$ photocatalyst for five consecutive cycles (**a**), XRD pattern of $BiVO_4/NH_4F$ before and after cycling stability test (**b**) and active species trapping experiment of $BiVO_4$ using MB dye (**c**)

of EDTA, t-BuOH and BQ quenchers the degradation percentage of MB reduces from 77 to 24% (h^+), 35% ($OH^\bullet$) and 47% ($O_2^{-\bullet}$) respectively. This decomposition demonstrates that h^+, $OH^\bullet$ and $O_2^{-\bullet}$ are primary reactive species involved for better photocatalytic performance of $BiVO_4/NH_4F$ photocatalysts.

3.10 *Photocatalytic Mechanism of $BiVO_4$*

The transportation of photo-generated charge carriers can be assumed through relative band potentials; these are valence and conduction band of semiconductors. In semiconductors, the conduction and valance band potential can be calculated by using formula:

$$E_{VB} = X - E_e + 0.5E_g \tag{3}$$

$$E_{CB} = E_{VB} - E_g \tag{4}$$

Here, E_{VB} and E_{CB} describe valance band and conduction band potentials of semiconductor. While E_g called "band gap energy of semiconductor." "E_e" is energy of free electron on hydrogen scale. *X* describes electronegativity of semiconductor and its value in the case of $BiVO_4$ is 6.04 eV (Chen et al., 2020). The determined values of valance and conduction band potentials for pristine $BiVO_4$, $BiVO_4$/oxalic acid, $BiVO_4$/CTAB, and $BiVO_4/NH_4F$ are mentioned in Table 3. Figure 11 exposes the mechanism of charge

Table 3 Values of band gap energy, valance band and conduction band of prepared materials

Sr. #	Material name	Band gap (eV)	Valance band (eV)	Conduction band (eV)
1	Pure $BiVO_4$	2.41	2.75	0.34
2	$BiVO_4$/oxalic acid	2.39	2.73	0.34
3	$BiVO_4$/CTAB	2.37	2.73	0.36
4	$BiVO_4$/ammonium fluoride	2.44	2.76	0.32

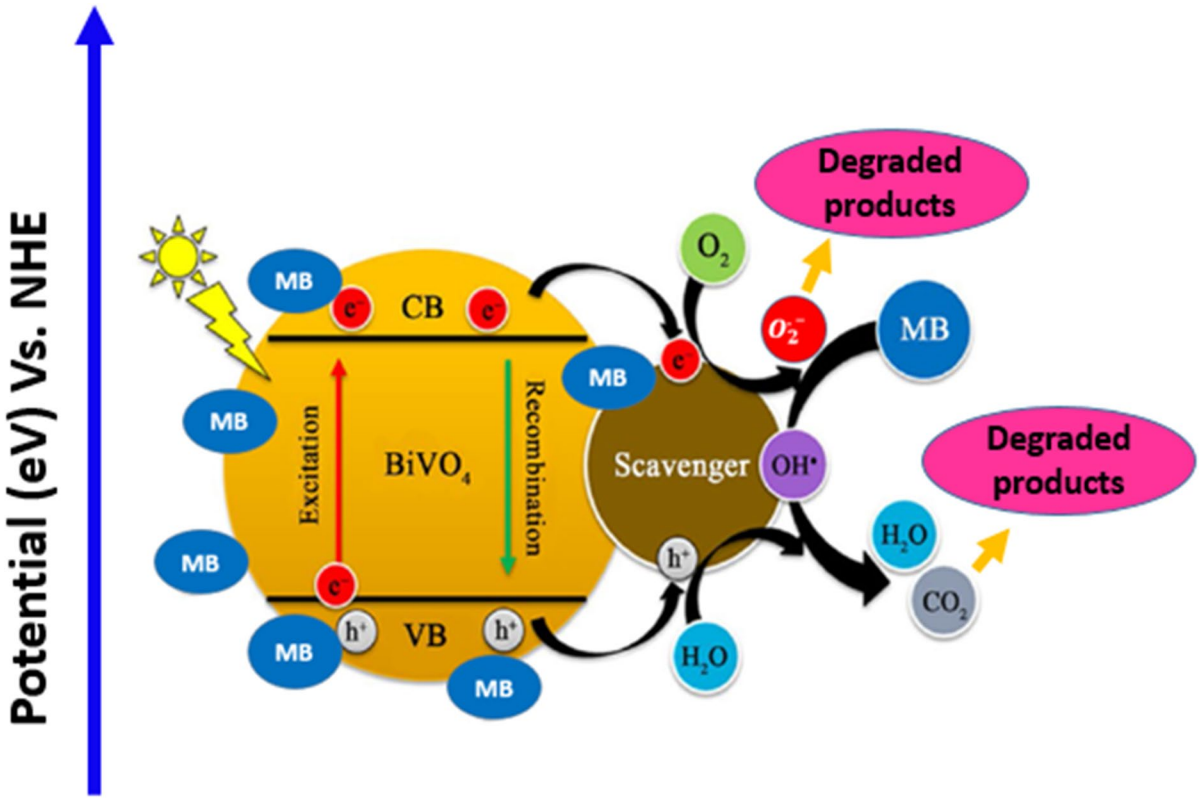

Fig. 11 Photocatalytic reaction mechanism of $BiVO_4$ nanocomposite for enhanced photocatalytic activity

transfer through photocatalytic degradation of MB dye. When light falls on $BiVO_4$, the photogenerated electrons from the valence band of $BiVO_4$ can be easily transferred towards conduction band leaving behind the holes in the valance band. The holes produced in valance band react with water molecules to create hydroxyl radicals that are capable of degrading the methylene blue dye molecules. Simultaneously, photogenerated electrons from the conduction band participated in oxidation reaction to generate superoxide radicals ($O_2^{-\bullet}$). Hence, hydroxyl radicals and superoxide radicals were responsible for degradation of methylene blue dye into non-toxic organic compounds. The detailed mechanism is summarized as:

$$BiVO_4 + hv \rightarrow BiVO_4\left(e^- + h^+\right) \quad (5)$$

$$BiVO_4 + O_2 \rightarrow BiVO_4 + O_2^- \quad (6)$$

$$BiVO_4 + H_2O \rightarrow BiVO_4 + {}^{\cdot}OH + H^+ \quad (7)$$

$${}^{\cdot}OH + organic\ dyes \rightarrow Degradation\ products \quad (8)$$

Hence, the prepared $BiVO_4/NH_4F$ materials exhibit greater photocatalytic performance in case of MB due to its monoclinic phase, greater crystallinity, superior morphological and optical properties. Furthermore, it has suppressed recombination rate of photogenerated charge carriers during photocatalytic reactions. Moreover, the use of FTIR spectroscopy in photocatalysis is of greater importance because it describes the qualitative and quantitative molecular insights into the interfacial process occurring in adsorption/desorption and chemical reaction (Atitar, et al., 2015).

4 Conclusion

In summary, we have synthesized bismuth vanadate ($BiVO_4$) nanoparticles using a simple hydrothermal route by adding surfactants. Developed structural, morphological, and optical properties of prepared $BiVO_4$ nanomaterials were examined. These prepared $BiVO_4$ nanostructures had stronger intensity, greater crystallinity and multi-morphological characteristics with superior visible light to induce photocatalytic activity for degradation of MB and RhB dyes. It was also concluded that the $BiVO_4/NH_4F$ material as compared to other materials show greater structural, morphological, optical properties and suppressed recombination rate which consequently resulted in enhanced photocatalytic activity. In addition, the hydrothermal method enables the production of excess interfacial $\cdot OH$ radicals on $BiVO_4$ particles promoting reactions between electrons and adsorbed species on $BiVO_4$ particles. The adsorbed species are O_2 and H_2O stop the photoexcited electrons and holes from recombining facilitating photocatalytic decomposition. Finally, the modified $BiVO_4$ will be a potential material for photocatalytic activity and elimination of pollutants.

Data Availability All data generated or analyzed during this study are included in this published article.

Declarations

Conflict of Interest The authors declare no competing interests.

References

Afonso, R., et al. (2014). Photoelectroactivity of bismuth vanadate prepared by combustion synthesis: Effect of different fuels and surfactants. *Journal of the Brazilian Chemical Society, 25*(4), 726–733.

Aghakhaninejad, S., R. Rahimi, and S. Zargari. *Application of BiVO4 nanocomposite for photodegradation of methyl orange*. in *Multidisciplinary Digital Publishing Institute Proceedings*. 2018.

Ahmed, T., et al. (2018). Surfactant-free synthesis of m-BiVO4 nanoribbons and enhanced visible-light photocatalytic properties. *Materials Research Bulletin, 99*, 298–305.

Atitar, M.F., et al., (2015) *The relevance of ATR-FTIR spectroscopy in semiconductor photocatalysis*. InTech.

Benisti, I., et al. (2020). Nanoseconds-resolved transient FTIR spectroscopy as a tool for studying the photocatalytic behavior of various types of bismuth vanadate. *Applied Catalysis B: Environmental, 278*, 119351.

Bhowmick, G., et al. (2019). Improved wastewater treatment by combined system of microbial fuel cell with activated carbon/TiO 2 cathode catalyst and membrane bioreactor. *Journal of the Institution of Engineers (india): Series A, 100*(4), 675–682.

Brack, P., et al. (2015). Aerosol-assisted CVD of bismuth vanadate thin films and their photoelectrochemical properties. *Chemical Vapor Deposition, 21*(1-2–3), 41–45.

Chang, S.-M., & Liu, W.-S. (2011). Surface doping is more beneficial than bulk doping to the photocatalytic activity of vanadium-doped TiO2. *Applied Catalysis B: Environmental, 101*(3–4), 333–342.

Chen, F.-Y., et al. (2020). Facile and rapid synthesis of a novel spindle-like heterojunction BiVO 4 showing enhanced visible-light-driven photoactivity. *RSC Advances, 10*(9), 5234–5240.

Cheng B., et al., (2012) One-pot template-free hydrothermal synthesis of monoclinic BiVO 4 hollow microspheres and their enhanced visible-light photocatalytic activity. International Journal of Photoenergy

Cheng, Y., et al. (2013). Preparation of porous BiVO 4 fibers by electrospinning and their photocatalytic performance under visible light. *RSC Advances, 3*(43), 20606–20612.

Cheng, Y., et al. (2020). A facile photoelectrochemical sensor for high sensitive dopamine and ascorbic acid detection based on bi surface plasmon resonance-promoted BiVO4 microspheres. *Journal of the Electrochemical Society, 167*(2), 027536.

Choi, S. K., Choi, W., & Park, H. (2013). Solar water oxidation using nickel-borate coupled BiVO 4 photoelectrodes. *Physical Chemistry Chemical Physics, 15*(17), 6499–6507.

Dabodiya, T. S., Selvarasu, P., & Murugan, A. V. (2019). Tetragonal to monoclinic crystalline phases change of BiVO4 via microwave-hydrothermal reaction: In correlation with visible-light-driven photocatalytic performance. *Inorganic Chemistry, 58*(8), 5096–5110.

Deebasree, J., et al. (2020). Effect of ultrasonication during and after preparation of BiVO4 by chemical coprecipitation technique. *Materials Today: Proceedings, 23*, 131–138.

Ganeshbabu, M., et al. (2020). Synthesis and characterization of BiVO 4 nanoparticles for environmental applications. *RSC Advances, 10*(31), 18315–18322.

García-Pérez, U., et al. (2012). Selective synthesis of monoclinic bismuth vanadate powders by surfactant-assisted co-precipitation method: Study of their electrochemical and photocatalytic properties. *International Journal of Electrochemical Science, 7*, 9622–9632.

Ghotekar, S., et al. (2020). A review on eco-friendly synthesis of BiVO4 nanoparticle and its eclectic applications. *Advanced Journal of Science and Engineering, 1*(4), 106–112.

Helal, A., et al., (2020) Novel synthesis of BiVO4 using homogeneous precipitation and its enhanced photocatalytic activity. Journal of Nanoparticle Research, 22(6).

Hemavibool, K., Sansenya, T., & Nanan, S. (2022). Enhanced photocatalytic degradation of tetracycline and oxytetracycline antibiotics by BiVO4 photocatalyst under visible light and solar light irradiation. *Antibiotics, 11*(6), 761.

Hunge, Y. M., et al. (2021). Visible light-assisted photocatalysis using spherical-shaped bivo4 photocatalyst. *Catalysts, 11*(4), 460.

Jia, Q., Iwashina, K., & Kudo, A. (2012). Facile fabrication of an efficient BiVO4 thin film electrode for water splitting under visible light irradiation. *Proceedings of the National Academy of Sciences, 109*(29), 11564–11569.

Jiang, G., et al. (2012). Novel highly active visible-light-induced photocatalysts based on BiOBr with Ti doping and Ag decorating. *ACS Applied Materials & Interfaces, 4*(9), 4440–4444.

Jiang, G., et al. (2014). Immobilization of N, S-codoped BiOBr on glass fibers for photocatalytic degradation of rhodamine B. *Powder Technology, 261*, 170–175.

Kása, Z., et al. (2020). New insights into the photoactivity of shape-tailored BiVO4 semiconductors via photocatalytic degradation reactions and classical reduction processes. *Molecules, 25*(20), 4842.

Kaur, K., et al. (2020). Photodegradation of organic pollutants using heterojunctions: A review. *Journal of Environmental Chemical Engineering, 8*(2), 103666.

Khan, I., et al. (2020). Ultrasonically controlled growth of monodispersed octahedral BiVO4 microcrystals for improved photoelectrochemical water oxidation. *Ultrasonics Sonochemistry, 68*, 105233.

Khan, I., et al., (2020) Ultrasonically controlled growth of monodispersed octahedral BiVO4 microcrystals for improved photoelectrochemical water oxidation. UltrasonicsSonochemistry, 105233.

Kshetri, Y. K., et al. (2020). Microwave hydrothermal synthesis and upconversion properties of BiVO4 nanoparticles. *Nanotechnology, 31*(24), 244001.

Kumar, S., et al. (2018). ZnO-graphene quantum dots heterojunctions for natural sunlight-driven photocatalytic environmental remediation. *Applied Surface Science, 447*, 802–815.

Li, W., et al. (2016). Relationship between crystalline phases and photocatalytic activities of BiVO4. *Materials Research Bulletin, 83*, 259–267.

Li, S., et al. (2020). Design, fabrication and characterization of photocatalyst Ni-doped BiVO4 for high effectively degrading dye contaminant. *Materials Research Express, 7*(11), 115005.

Liaqat, M., & Khalid, N. (2021). Efficient photocatalysis performance and recyclability of MoO3/BiVO4 heterostructure under visible light. *Applied Nanoscience, 11*(7), 2085–2094.

Liaqat, M., et al. (2022). Fabrication of novel BiVO4/Bi2O3 heterostructure with superior visible light induced photocatalytic properties. *Nanotechnology, 34*(1), 015711.

Liaqat, M., et al. (2023). Visible light induced photocatalytic activity of MnO2/BiVO4 for the degradation of organic dye and tetracycline. *Ceramics International, 49*(7), 10455–10461.

Lin, Y., Lu, C., & Wei, C. (2019). Microstructure and photocatalytic performance of BiVO4 prepared by hydrothermal method. *Journal of Alloys and Compounds, 781*, 56–63.

Liu, Y., et al. (2018). Enhanced photocatalytic activity over flower-like sphere Ag/Ag2CO3/BiVO4 plasmonic heterojunction photocatalyst for tetracycline degradation. *Chemical Engineering Journal, 331*, 242–254.

Lotfi, S., et al., Recent progress on the synthesis, morphology and photocatalytic dye degradation of BiVO4 photocatalysts: a review. Catalysis Reviews, 2022: 1–45.

Luo, Y., et al. (2022a). Ball-milled bismuth oxybromide/biochar composites with enhanced removal of reactive red owing to the synergy between adsorption and photodegradation. *Journal of Environmental Management, 308*, 114652.

Luo, Y., et al. (2022b). Step scheme nickel-aluminium layered double hydroxides/biochar heterostructure photocatalyst for synergistic adsorption and photodegradation of tetracycline. *Chemosphere, 309*, 136802.

Luo, Y., et al. (2023). Integrated adsorption and photodegradation of tetracycline by bismuth oxycarbonate/biochar nanocomposites. *Chemical Engineering Journal, 457*, 141228.

Malathi, A., et al. (2018). A review on BiVO4 photocatalyst: Activity enhancement methods for solar photocatalytic applications. *Applied Catalysis a: General, 555*, 47–74.

Mao, J., et al. (2020). Facile fabrication of porous BiVO 4 hollow spheres with improved visible-light photocatalytic properties. *RSC Advances, 10*(11), 6395–6404.

Monfort, O., & Plesch, G. (2018). Bismuth vanadate-based semiconductor photocatalysts: A short critical review on the efficiency and the mechanism of photodegradation of organic pollutants. *Environmental Science and Pollution Research, 25*(20), 19362–19379.

Mousavi-Kamazani, M. (2019). Facile hydrothermal synthesis of egg-like BiVO 4 nanostructures for photocatalytic desulfurization of thiophene under visible light irradiation. *Journal of Materials Science: Materials in Electronics, 30*(19), 17735–17740.

Nguyen, T.D., et al., (2020) BiVO 4 photocatalysis design and applications to oxygen production and degradation of organic compounds: a review. Environmental Chemistry Letters, 1–23.

Ran, R., J.G. McEvoy, and Z. Zhang (2015) Synthesis and optimization of visible light active BiVO4 photocatalysts for the degradation of RhB. International Journal of Photoenergy, 2015.

Rani, B. J., et al. (2018). Ferrimagnetism in cobalt ferrite (CoFe2O4) nanoparticles. *Nano-Structures & Nano-Objects, 14*, 84–91.

Rani, B. J., et al. (2019). BiVO4 nanostructures for photoelectrochemical (PEC) solar water splitting applications. *Journal of Nanoscience and Nanotechnology, 19*(11), 7427–7435.

Reddy, C.V., et al., (2023) Novel g-C3N4/BiVO4 heterostructured nanohybrids for high efficiency photocatalytic degradation of toxic chemical pollutants. Chemosphere, 138146.

Sajid, M. M., et al. (2020). Generation of strong oxidizing radicals from plate-like morphology of BiVO 4 for the fast degradation of crystal violet dye under visible light. *Applied Physics A, 126*, 1–12.

Senasu, T., et al. (2021). Sunlight-driven photodegradation of oxytetracycline antibiotic by BiVO4 photocatalyst. *Journal of Solid State Chemistry, 297*, 122088.

Sivakumar, V., et al. (2015). BiVO4 nanoparticles: Preparation, characterization and photocatalytic activity. *Cogent Chemistry, 1*(1), 1074647.

Tayebi, M., & Lee, B.-K. (2019). Recent advances in BiVO4 semiconductor materials for hydrogen production using photoelectrochemical water splitting. *Renewable and Sustainable Energy Reviews, 111*, 332–343.

Trinh, D. T. T., et al. (2019). Synthesis, characterization and environmental applications of bismuth vanadate. *Research on Chemical Intermediates, 45*(10), 5217–5259.

Wang, T., et al. (2014). Reduced graphene oxide (rGO)/BiVO4 composites with maximized interfacial coupling for visible lght photocatalysis. *ACS Sustainable Chemistry & Engineering, 2*(10), 2253–2258.

Wu, M., et al. (2018). BiVO4 microstructures with various morphologies: Synthesis and characterization. *Applied Surface Science, 427*, 525–532.

Wu, H., et al. (2021). Unveiling carrier dynamics in periodic porous BiVO4 photocatalyst for enhanced solar water splitting. *ACS Energy Letters, 6*(10), 3400–3407.

You, J., et al. (2019). A review of visible light-active photocatalysts for water disinfection: Features and prospects. *Chemical Engineering Journal, 373*, 624–641.

Yu, J., & Kudo, A. (2006). Effects of structural variation on the photocatalytic performance of hydrothermally synthesized BiVO4. *Advanced Functional Materials, 16*(16), 2163–2169.

Zhang, A., & Zhang, J. (2009). Characterization of visible-light-driven BiVO4 photocatalysts synthesized via a surfactant-assisted hydrothermal method. *Spectrochimica Acta Part a: Molecular and Biomolecular Spectroscopy, 73*(2), 336–341.

Zhang, X., et al. (2007). Selective synthesis and visible-light photocatalytic activities of BiVO4 with different crystalline phases. *Materials Chemistry and Physics, 103*(1), 162–167.

Zhang, Y., et al. (2014). Facile synthesis of V 4+ self-doped,[010] oriented BiVO 4 nanorods with highly efficient visible light-induced photocatalytic activity. *Physical Chemistry Chemical Physics, 16*(44), 24519–24526.

Zhang, T., et al. (2020). Bacitracin-assisted synthesis of spherical BiVO 4 nanoparticles with C doping for remarkable photocatalytic performance under visible light. *CrystEngComm, 22*(10), 1812–1821.

Zhang, X., et al. (2021). Performance and mechanism of biochar-coupled BiVO4 photocatalyst on the degradation of sulfanilamide. *Journal of Cleaner Production, 325*, 129349.

Zhong, X., et al. (2023). Recent progress in BiVO4-based heterojunction nanomaterials for photocatalytic applications. *Materials Science and Engineering: B, 289*, 116278.

Zhou, L., et al. (2006). A sonochemical route to visible-light-driven high-activity BiVO4 photocatalyst. *Journal of Molecular Catalysis a: Chemical, 252*(1–2), 120–124.

Zhou, L., et al. (2007). Single-crystalline BiVO4 microtubes with square cross-sections: Microstructure, growth mechanism, and photocatalytic property. *The Journal of Physical Chemistry C, 111*(37), 13659–13664.